

1 **Interpretation of NO₃-N₂O₅ observation via steady state in high aerosol air**
2 **mass: The impact of equilibrium coefficient in ambient conditions**

3 Xiaorui Chen¹, Haichao Wang^{3,4}, Keding Lu^{1,2}

4 ¹State Key Joint Laboratory of Environmental Simulation and Pollution Control, College of
5 Environmental Sciences and Engineering, Peking University, Beijing, China.

6 ²The State Environmental Protection Key Laboratory of Atmospheric Ozone Pollution Control,
7 College of Environmental Sciences and Engineering, Peking University, Beijing, China

8 ³School of Atmospheric Sciences, Sun Yat-sen University, Zhuhai, 519082, China

9 ⁴Guangdong Provincial Observation and Research Station for Climate Environment and Air
10 Quality Change in the Pearl River Estuary, Key Laboratory of Tropical Atmosphere-Ocean
11 System, Ministry of Education, Southern Marine Science and Engineering Guangdong
12 Laboratory (Zhuhai), Zhuhai, 519082, China

13 *Correspondence to:* Haichao Wang (wanghch27@mail.sysu.edu.cn), Keding Lu
14 (k.lu@pku.edu.cn)

15

16 **Abstract.** Steady state approximation for interpreting NO₃ and N₂O₅ has large uncertainty
17 under complicated ambient conditions and could even produces incorrect results
18 unconsciously. To provide an assessment and solution to the dilemma, we formulate data sets
19 based on in-situ observations to reassess the applicability of the method. In most of steady
20 state cases, we find a prominent discrepancy between K_{eq} (equilibrium coefficient for
21 reversible reactions of NO₃ and N₂O₅) and correspondingly simulated $[N_2O_5]/([NO_2] \times [NO_3])$,
22 especially under high aerosol conditions in winter. This gap reveals the accuracy of K_{eq} has a
23 critical impact on the steady state analysis in polluted region. In addition, the accuracy of
24 $\gamma(N_2O_5)$ derived by steady state fit depends closely on the reactivity of NO₃ (k_{NO_3}) and N₂O₅
25 ($k_{N_2O_5}$). Based on a complete set of simulations, air mass of k_{NO_3} less than 0.01 s⁻¹ with high
26 aerosol and temperature higher than 10°C is suggested to be the best suited for steady state
27 analysis of NO₃-N₂O₅ chemistry. Instead of confirming the validity of steady state by
28 numerical modeling for every case, this work directly provides appropriate concentration
29 ranges for accurate steady state approximation, with implications for choosing suited methods
30 to interpret nighttime chemistry in high aerosol air mass.

31

32 1 Introduction

33 Nitrate radical (NO_3), an extremely reactive species prone to build up at night, is an ideal
 34 candidate for steady state analysis in combine with dinitrogen pentoxide (N_2O_5) due to fast
 35 equilibrium reactions between them (R1).



36 Under the steady state condition, the lifetime of NO_3 (denoted as $\tau_{ss}(\text{NO}_3)$) can be
 37 calculated as the ratio of NO_3 concentration over the production rate ($k_{\text{NO}_2+\text{O}_3}[\text{NO}_2][\text{O}_3]$) or
 38 over the removal rate of both NO_3 and N_2O_5 , as indicated in Eq. (1). A similar representation
 39 of N_2O_5 steady state lifetime is also shown in Eq. (2). The loss frequencies of various sink
 40 pathways of NO_3 and N_2O_5 are integrated as total first-order in the following equations,
 41 represented by k_{NO_3} and $k_{\text{N}_2\text{O}_5}$ term. Briefly, the k_{NO_3} is contributed by the reaction of NO_3
 42 radical with NO and hydrocarbons and uptake on particles at night, ranging from hundredths
 43 of s^{-1} to several s^{-1} depending on the air mass. Due to its large rate constant with NO, the
 44 concentration usually dominates the lifetime of NO_3 radical in urban areas with fresh NO
 45 emission. Otherwise, the reactions with hydrocarbons, especially unsaturated hydrocarbons,
 46 is preferential for NO_3 in rural areas. The K_{eq} denotes the equilibrium coefficient for reactions
 47 R1a and R1b, used to be derived by Eq. (3).

$$48 \quad \tau_{ss}(\text{NO}_3) \equiv \frac{[\text{NO}_3]}{k_{\text{NO}_2+\text{O}_3}[\text{NO}_2][\text{O}_3]} \approx (k_{\text{NO}_3} + K_{eq}[\text{NO}_2]k_{\text{N}_2\text{O}_5})^{-1}, \quad (1)$$

$$49 \quad \tau_{ss}(\text{N}_2\text{O}_5) \equiv \frac{[\text{N}_2\text{O}_5]}{k_{\text{NO}_2+\text{O}_3}[\text{NO}_2][\text{O}_3]} \approx (k_{\text{N}_2\text{O}_5} + \frac{k_{\text{NO}_3}}{K_{eq}[\text{NO}_2]})^{-1}, \quad (2)$$

$$50 \quad K_{eq} = \frac{k_{\text{R1a}}}{k_{\text{R1b}}} = \frac{[\text{N}_2\text{O}_5]}{[\text{NO}_2][\text{NO}_3]}, \quad (3)$$

51 Numerous works have taken the advantage of the steady state calculation to quantify the total
 52 first-order loss rate for NO_3 or N_2O_5 such that they drew conclusions about the oxidation
 53 capacity and reactive nitrogen budgets contributed by this chemical system (Allan et al.,
 54 1999; Allan et al., 2000; Carslaw et al., 1997; Platt et al., 1984; Vrekoussis et al., 2007; Wang et
 55 al., 2013). Since the steady state approximation was used to interpret atmospheric observation
 56 of NO_3 - N_2O_5 (Brown, 2003; Platt et al., 1981), this method was also widely implemented to
 57 quantify N_2O_5 uptake coefficient ($\gamma(\text{N}_2\text{O}_5)$) (Brown et al., 2009; Brown et al., 2003; Li et al.,
 58 2020; McDuffie et al., 2019; Phillips et al., 2016; Wang et al., 2017a; Wang et al., 2017c; Wang
 59 et al., 2020a).

60 However, with the influence induced by complicated atmospheric conditions and
 61 emission, the steady state in ambient air mass will not always be the case (as illustrated in Text

62 S1 and Figure S1). These situations are prevalent in nocturnal boundary layer (Phillips et al.,
63 2016;Stutz et al., 2004;Wang et al., 2017a;Wang et al., 2017c) and therefore increase the
64 difficulty of applying steady state directly on NO₃-N₂O₅ observation data, whereas few studies
65 have systematically characterized the error source and application conditions of this method
66 (Brown et al., 2009).

67 Due to faster approach to equilibrium than steady state, the application of K_{eq} in
68 calculation steady state equations seems to be reasonable (Brown et al., 2003). For example,
69 the ambient NO₃ concentration was usually calculated based on ambient N₂O₅ concentration
70 with $K_{eq} \times [NO_2]$ when determining their budgets or characterizing the lifetime or sink
71 attribution of these two reactive nitrogen compounds (Brown et al., 2011;Osthoff et al.,
72 2006;Wang et al., 2018;Wang et al., 2017c;Wang et al., 2017d;Yan et al., 2019). In addition,
73 the mathematical conversion between NO₃ and N₂O₅ concentration via K_{eq} coefficient can
74 simplified the calculation in the iterative box model, which derives $\gamma(N_2O_5)$ by iterating its
75 value in the model until the predicted N₂O₅ concentration matches the observation (Wagner et
76 al., 2013;Wang et al., 2020b). However, considerable uncertainty could be associated with the
77 quantification of K_{eq} and its different parameterizations (Cantrell et al., 1988;Pritchard, 1994).
78 The impact of K_{eq} value on steady state fit or concentration conversion have not been explored
79 to date in the analysis of NO₃-N₂O₅ steady state.

80 In this study, we formulate a half artificial dataset with expected properties based on field
81 campaigns. Specifically, most of species contained in the dataset are observed values while
82 only NO₃ and N₂O₅ were calculated by the steady state model (illustrated in the section 2.2).
83 With the dataset, we illustrate the reasons for deviation of parameterized K_{eq} from
84 $[N_2O_5]/([NO_2] \times [NO_3])$ in ambient conditions, the possible uncertainties of linear fit based on
85 steady state equations Eq. (4) and Eq. (5) (the related variables are explained in section 2.1)
86 resulted from different K_{eq} , and the influence of relevant atmospheric variables on $\gamma(N_2O_5)$
87 derivation via steady state method. Furthermore, a series of ambient condition tests specify
88 the exact ranges suited for steady state analysis according to not only the validity of steady
89 state but also K_{eq} values, which optimizes the validity check by numerical modeling in
90 previous research (Brown et al., 2009;Brown et al., 2003) and develops complete standard for
91 data filtering.

92 2 Methods

93 2.1 $\gamma(\text{N}_2\text{O}_5)$ derivation by steady state approximation

94 The framework of steady state approximation for NO_3 - N_2O_5 system is basically built on its
95 chemical production and removal pathways, in case of extremely weak physical processes (e.g.
96 transport, dilution and deposition) relative to its chemical processes. With simultaneous
97 measurements of NO_3 , N_2O_5 and relevant precursor concentrations, the steady state lifetime
98 $\tau_{ss}(\text{NO}_3)$ and $\tau_{ss}(\text{N}_2\text{O}_5)$ can be quantified for a targeted period as shown in Eq. (1) and Eq.
99 (2). By substituting the $k\text{N}_2\text{O}_5$ with $0.25 \times c \times S_a \times \gamma(\text{N}_2\text{O}_5)$, the $\gamma(\text{N}_2\text{O}_5)$ and the reactivity of NO_3
100 ($k\text{NO}_3$, including the reactions of NO_3 with NO and hydrocarbons) can therefore be
101 determined by Eq. (4) and Eq. (5).

$$102 \tau_{ss}^{-1}(\text{NO}_3) \approx k_{\text{NO}_3} + 0.25cS_aK_{eq}[\text{NO}_2]\gamma(\text{N}_2\text{O}_5), \quad (4)$$

$$103 (0.25cS_a\tau_{ss}(\text{N}_2\text{O}_5))^{-1} \approx \gamma(\text{N}_2\text{O}_5) + k_{\text{NO}_3}(0.25cS_aK_{eq}[\text{NO}_2])^{-1}, \quad (5)$$

104 Here c represents the mean molecular velocity of N_2O_5 , S_a represents the aerosol surface area
105 and the K_{eq} is calculated from the rate constant of reversible reactions R1a (k_{R1a}) and R1b
106 (k_{R1b}), which is a temperature-dependent parameter. It should be noted that the photolysis of
107 NO_3 is not considered in the $k\text{NO}_3$ due to weak radiation at night and the homogeneous
108 hydrolysis was also ignored due to its small contribution in comparison to heterogeneous
109 pathway, similar presumption was also implemented in previous studies (Brown et al.,
110 2009; Mentel et al., 1996; Wahner et al., 1998). In the form of these two equations, the potential
111 covariance between S_a and NO_2 concentration can be avoided to decrease the uncertainty
112 (Brown et al., 2009). By fit to these two equations, $\gamma(\text{N}_2\text{O}_5)$ can be directly derived from slope
113 of the plot of $\tau_{ss}^{-1}(\text{NO}_3)$ against $0.25cS_aK_{eq}[\text{NO}_2]$ or from intercept of the plot of
114 $(0.25cS_a\tau_{ss}(\text{N}_2\text{O}_5))^{-1}$ against $(0.25cS_aK_{eq}[\text{NO}_2])^{-1}$ respectively. In the following
115 analysis, the linear fit based on Eq. (5) is preferred in steady state approximation.

116 2.2 Steady state model and half-artificial datasets

117 The steady state model is reformed from 0-dimension box model to produce NO_3 and N_2O_5
118 which are in steady state as far as possible. It is constrained by measurements of NO , NO_2 ,
119 O_3 , CO , CH_4 , VOCs, HCHO, S_a , relative humidity (RH), temperature (T), pressure, coupled
120 with Regional Atmospheric Chemistry Mechanism, version 2 (RACM2). Each data point is
121 treated as an independent air mass, aging 10 hours and keeping input constraint unchanged.
122 As NO_3 - N_2O_5 chemistry, the interest of this work, usually shows marked impacts during the
123 night, only the time periods with negligible photolysis frequency are under consideration. In

124 the standard simulation (herein referred as Mod0), the uptake coefficient of N₂O₅ is set to 0.02,
125 as a reasonable value of literatures (Brown et al., 2006;Chen et al., 2020;McDuffie et al.,
126 2018;Morgan et al., 2015;Phillips et al., 2016;Wagner et al., 2013;Wang et al., 2017c;Yu et al.,
127 2020).

128 Two half-artificial datasets are derived from PKU2017 and TZ2018 field campaigns (see
129 Text S2) based on steady state model for analysis in the following sections. The simulated NO₃
130 and N₂O₅ and other observed values used for the constraints of steady state model jointly
131 formulate these half-artificial datasets. Specifically, the NO₃ and N₂O₅ concentration in this
132 dataset are the output of the steady state model simulation, and guaranteed to be in steady state
133 with respect to other observed precursors. To verify the steady state of NO₃ and N₂O₅ for each
134 data point, we filtered the data set according to deviation between steady state lifetime of N₂O₅
135 ($\tau_{ss}(N_2O_5) = \frac{[N_2O_5]}{k_{R1}[NO_2][O_3]}$) and calculated lifetime of N₂O₅ ($\tau_{calc}(N_2O_5) = (k_{N_2O_5} +$
136 $\frac{k_{NO_3}}{K_{eq}[NO_2]})^{-1}$). If the deviation exceeds 10% for a data point, it will be excluded from the
137 following analysis. We presume that if any data point outputted from the model is still out of
138 steady state in terms of NO₃ and N₂O₅, the sink rate constant of air mass represented by this
139 data point should be too weak for steady state analysis within a reasonable timescale. In
140 addition, the data higher than 5 ppbv NO is filtered out in the following calculation, since the
141 resulting large variation of k_{NO_3} can bias the linear fit even though the NO₃ and N₂O₅
142 approach the steady state rapidly under high NO (discussed in 3.2). The fraction of excluded
143 data is less than 8%, which are expected to have little influence on our results. The calculated
144 nighttime loss fraction accounted by NO₃ and N₂O₅ show large discrepancy (see Text. S3 and
145 Figure S2) between these two half-artificial datasets, which provide us a good opportunity to
146 investigate the impacting factors on steady state approximation across different conditions.

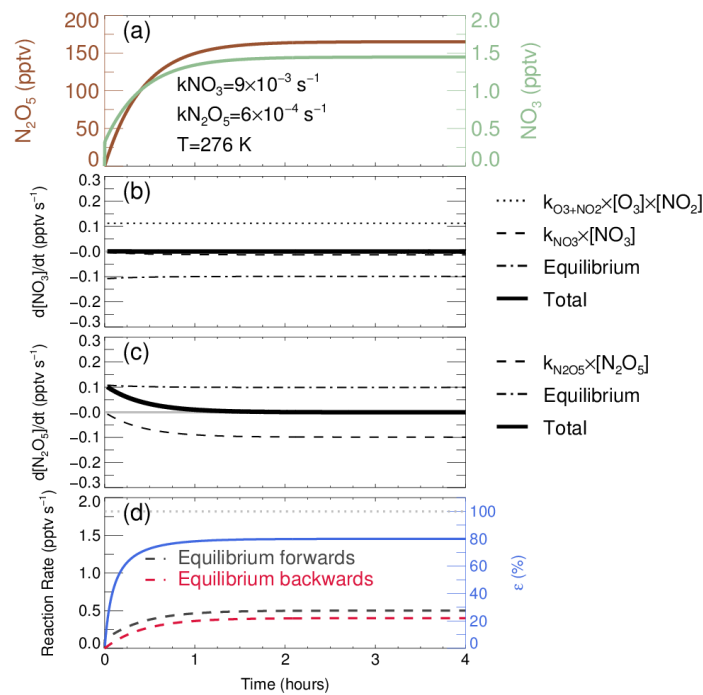
147 Rather than using observation data directly, a half-artificial dataset can provide larger
148 amount of valid data for steady state analysis with known $\gamma(N_2O_5)$ value. Besides, this method
149 avoids the impacts from steady state deviation, which helps to analyze the factors influencing
150 $\gamma(N_2O_5)$ quantification via steady state approximation backwards from a known steady state
151 condition.

152 **3 Results and discussion**

153 **3.1 Varying equilibrium coefficient under steady state**

154 The rates of NO₃-N₂O₅ reversible reactions are expected to be equal for the steady state case,
155 so that the equilibrium coefficient K_{eq} can be determined from either the rate constant ratio of
156 R1a and R1b or the ratio of $[N_2O_5]/([NO_2] \times [NO_3])$. Although this approach is reasonable

157 under ideal conditions, the exactly same rates between reversible reactions and the following
 158 calculation based on K_{eq} scaling are not so appropriate for ambient atmosphere where the
 159 removal pathway for $\text{NO}_3\text{-N}_2\text{O}_5$ are not negligible, especially under the high aerosol loading
 160 condition. The $\text{NO}_3\text{-N}_2\text{O}_5$ achieves steady state after 1.5-hours evolution, when concentration
 161 and rates remain constant (Figure 1). In this simulation, the starting mixing ratios of NO_2 and
 162 O_3 are 10 and 23 ppbv respectively, which is the average level for the nighttime conditions in
 163 PKU2017. The concentration of these two precursors are held constant in the simulation to
 164 better illustrate the influence of removal rates. This result will stay almost the same no matter
 165 these starting values are initialized to be constant or allowed to vary. Under steady state, the
 166 net equilibrium reaction rate in Figure 1(b)&(c) stays negative and positive for NO_3 and N_2O_5
 167 respectively. Besides, the absolute values and difference of the forward and backward reaction
 168 rates remain unchanged after achieving steady state. This result is similar with a previous
 169 numerical calculation study (Brown et al., 2003), while the deviation between reversible
 170 reaction rates becomes larger in our case.

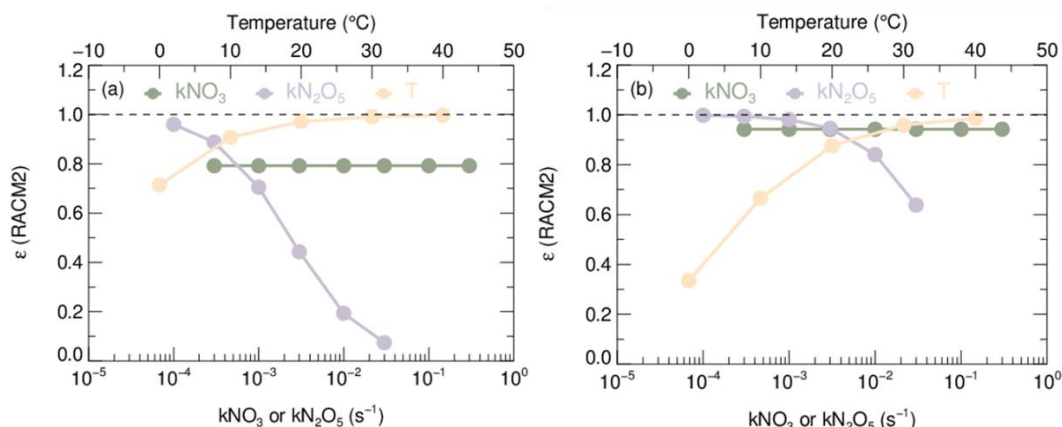


171
 172 **Figure 1.** Evolution of $\text{NO}_3\text{-N}_2\text{O}_5$ system simulated by steady state model for an average case. (a) Temporal
 173 profiles of N_2O_5 and NO_3 , the constraint of simulation is displayed as the text; (b) Evolution of $d[\text{NO}_3]/dt$
 174 calculated from source of $k_{\text{O}_3+\text{NO}_2} \times [\text{O}_3] \times [\text{NO}_2]$, sink of $k_{\text{NO}_3} \times [\text{NO}_3]$ and equilibrium terms, detailed in
 175 the text; (c) Evolution of $d[\text{N}_2\text{O}_5]/dt$ calculated from equilibrium terms, sink of $k_{\text{N}_2\text{O}_5} \times [\text{N}_2\text{O}_5]$; (d) Forward
 176 (N_2O_5 formation) and backward (N_2O_5 decomposition) equilibrium rate are represented as black and red
 177 dash lines, the equilibrium completeness ε is calculated by the ratio of backward rate over forward rate,
 178 shown as blue full line.

179 In this case, the original equilibrium is imperfect realized (a perfect realization of the
 180 original equilibrium condition is that K_{eq} and the ratio of $[N_2O_5]/([NO_2] \times [NO_3])$ are
 181 equivalent as Eq. (6)), leading to errors on projection of NO_3 and N_2O_5 concentration via K_{eq}
 182 $\times [NO_2]$. In fact, we note that a new equilibrium between NO_3 and N_2O_5 is developed with
 183 constant but unequal rates. Under this new equilibrium condition, the ratio of R1b reaction
 184 rate (the red dash line in Figure1(d)) over R1a reaction rate (the black dash line in Figure1(d))
 185 can be regarded as the degree of approaching original equilibrium (the blue line in Figure1(d)).
 186 In addition, this value is also the ratio of $[N_2O_5]/([NO_2] \times [NO_3])$ against original K_{eq} ,
 187 therefore we defined this ratio as a correction factor ε , implemented to calculate accurate
 188 $[N_2O_5]/([NO_2] \times [NO_3])$ with significant N_2O_5 removal pathways. The value of K_{eq} after
 189 scaled by ε can be used for converting the concentration of NO_3 and N_2O_5 via Eq. (6):

$$190 \quad \varepsilon \times K_{eq} = \varepsilon \times \frac{k_{R1a}}{k_{R1b}} = \frac{[N_2O_5]}{[NO_2][NO_3]}, \quad (6)$$

191 Sensitivity tests are conducted to demonstrate the dependence of ε on relevant variables
 192 based on steady state model. The average ambient conditions observed at wintertime PKU site
 193 and summertime TZ site are taken as basic constraint for sensitivity tests (Table S2),
 194 respectively. By separately altering variables, such as NO_2 , O_3 , kN_2O_5 , kNO_3 and T , the
 195 sensitivity of ε value can be obtained as shown in Figure 2 and Figure S4. The ε value
 196 depends primarily on kN_2O_5 and T in both scenarios, where ε increases with T (approaching
 197 1 under relatively high T) and decreases with kN_2O_5 . In comparison, the ε value behaves
 198 insensitive to kNO_3 as well as NO_2 and O_3 concentration, at least within the range of reasonable
 199 ambient conditions. High kN_2O_5 is resulted from high aerosol events, usually occur in winter
 200 accompanied with low temperature and high relative humidity in some populated areas
 201 (Baasandorj et al., 2017;Huang et al., 2014;Wang et al., 2017b;Wang et al., 2014), further
 202 decreasing the accuracy of original K_{eq} values. It can be inferred that in order to accurately
 203 interpreting relationship of NO_3 and N_2O_5 , calculation relying on equilibrium equation and
 204 steady state approximation should consider the dependence of ε on ambient conditions.



205

206 **Figure 2.** Sensitivity plot of $k\text{NO}_3$, $k\text{N}_2\text{O}_5$ and Temperature (T) against coefficient ε . The trace of T is
 207 plotted against the upper horizontal axis and the traces of the other two parameters are plotted against the
 208 lower horizontal axis. (a) Basic model condition is according to typical winter condition of PKU2017; (b)
 209 Basic model condition is according to typical summer condition of TZ2018. Basic model conditions
 210 including $k\text{NO}_3$, $k\text{N}_2\text{O}_5$ and Temperature (T) are shown in Table S2. It should be noted that the provided
 211 ranges of each factor do not exactly equal to but encompass the ambient conditions encountered during the
 212 two campaigns.

213 Even if K_{eq} value serves as a good representation of the ratio of $[\text{N}_2\text{O}_5]/([\text{NO}_2] \times [\text{NO}_3])$
 214 or ε can be readily quantified on field, the discrepancy among different database in
 215 calculating K_{eq} still increase the uncertainties of $\text{NO}_3\text{-N}_2\text{O}_5$ calculation through steady state
 216 approximation or equilibrium, which has not been carefully considered. Here, we apply a set
 217 of uniform formulas to describing k_{R1a} and k_{R1b} (see Text. S4) from preferred values of several
 218 popular atmospheric chemistry mechanisms (Mozart, CB05, Saprc07, RACM2 and kinetic
 219 databases JPL2015 as well as IUPAC2017) and finally calculating K_{eq} . As is shown in Figure
 220 S5 and Figure S6, K_{eq} variations derived from these six different databases reflect
 221 considerable discrepancy from each other, especially in colder conditions. Because
 222 parameterized K_{eq} values are only dependent on ambient temperature, they continuously
 223 increase with time due to the decrease of temperature. In addition to discrepancy between
 224 different K_{eq} parameterizations, ε value varies dissimilarly with each K_{eq} , ranging from 70%
 225 to 90%. All these results demonstrate that, in most cases, K_{eq} values simply derived from
 226 existing database would fail to reproduce accurate relationship between NO_3 and N_2O_5 .

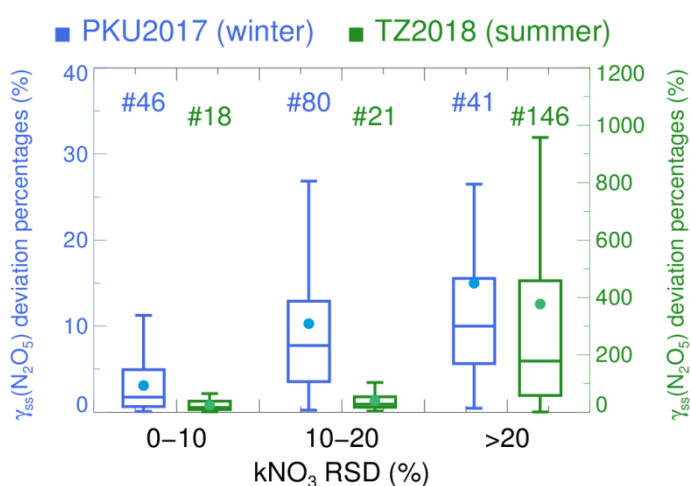
227 To further elucidate the impact of K_{eq} on deriving $\gamma(\text{N}_2\text{O}_5)$ via steady state approximation
 228 (hereafter defined as $\gamma_{\text{ss}}(\text{N}_2\text{O}_5)$), Figure S6 shows the steady state fit based on all six database-
 229 derived K_{eq} and in the same time periods as Figure S5 through Eq. (4) and Eq. (5) respectively
 230 (both of equations can derive a pair of $\gamma_{\text{ss}}(\text{N}_2\text{O}_5)$ and $k\text{NO}_3$). The K_{eq} (corrected with ε) is
 231 calculated with NO_3 and N_2O_5 concentration simulated based on RACM2. Fit based on Eq. (4)

232 could lead to 11~46% underestimation of $\gamma_{ss}(\text{N}_2\text{O}_5)$, as indicated by varying slopes in Figure
 233 S7(b)&(d), when using the database-derived K_{eq} . Conversely, fit by Eq. (5) (shown in Figure
 234 S7(a)&(c)) bias the result of $k\text{NO}_3$ served as the slopes without much influence on $\gamma_{ss}(\text{N}_2\text{O}_5)$
 235 served as the intercept. Previous research ascribed inconsistent fit results between two
 236 equations to measurements uncertainty (Brown et al., 2009; Brown et al., 2006). However, fit
 237 with original K_{eq} might be the primary reasons for such inconsistent results, and even deviates
 238 the derived $\gamma_{ss}(\text{N}_2\text{O}_5)$ and $k\text{NO}_3$ from true values. Therefore, steady state fit based on Eq. (5)
 239 might be the best choice for $\gamma(\text{N}_2\text{O}_5)$ derivation via steady state approximation. Similarly, Eq.
 240 (4) is preferred to be applied when $k\text{NO}_3$ is the final objective.

241 3.2 Impacts of $\text{NO}_3\text{-N}_2\text{O}_5$ reactivity on steady state

242 In order to further explore the impacting factors on steady state fit method, $\gamma_{ss}(\text{N}_2\text{O}_5)$ results
 243 are derived for each 2-hour time period of PKU2017 and TZ2018 dataset based on output from
 244 steady state model. Since the pre-set $\gamma(\text{N}_2\text{O}_5)$ in this model is 0.02, the degree of deviation
 245 from this value is supposed to reflect the accuracy of the fitted result.

246 It can be noticed from Eq. (5) that the variability of $k\text{NO}_3$ during the same time period
 247 leads data points to scatter on lines with different slopes, which could bias the resulted $\gamma_{ss}(\text{N}_2\text{O}_5)$
 248 from model pre-set value. As is shown in Figure 3, the absolute percentages of $\gamma_{ss}(\text{N}_2\text{O}_5)$
 249 deviation grow dramatically with the increase of relative standard deviation of $k\text{NO}_3$ ($k\text{NO}_3$
 250 RSD) in both of winter and summer data sets. The positive correlation even gives rise to
 251 extreme deviation in summer data set with up to almost 10 times of model setting $\gamma(\text{N}_2\text{O}_5)$. In
 252 fact, there remains accurate $\gamma_{ss}(\text{N}_2\text{O}_5)$ values derived in each range of $k\text{NO}_3$ RSD, indicating a
 253 not strictly positive correlation between $\gamma_{ss}(\text{N}_2\text{O}_5)$ deviation and $k\text{NO}_3$ RSD. It implies that
 254 large variation of $k\text{NO}_3$ only enhance the possibilities of inaccurate results from steady state
 255 fit rather than hinder the $\gamma_{ss}(\text{N}_2\text{O}_5)$ quantification all the time.



256

257 **Figure 3.** Relationship between $\gamma(\text{N}_2\text{O}_5)$ derivation through steady state approximation and $k\text{NO}_3$ relative
258 standard deviation (RSD) in box whisker plot. The blue and green color represent dataset from PKU2017
259 and TZ2018 respectively, binned according to $k\text{NO}_3$ RSD. The dots are the mean deviation of $\gamma_{\text{ss}}(\text{N}_2\text{O}_5)$.
260 The number above the box whisker represents the valid data points in each bin.

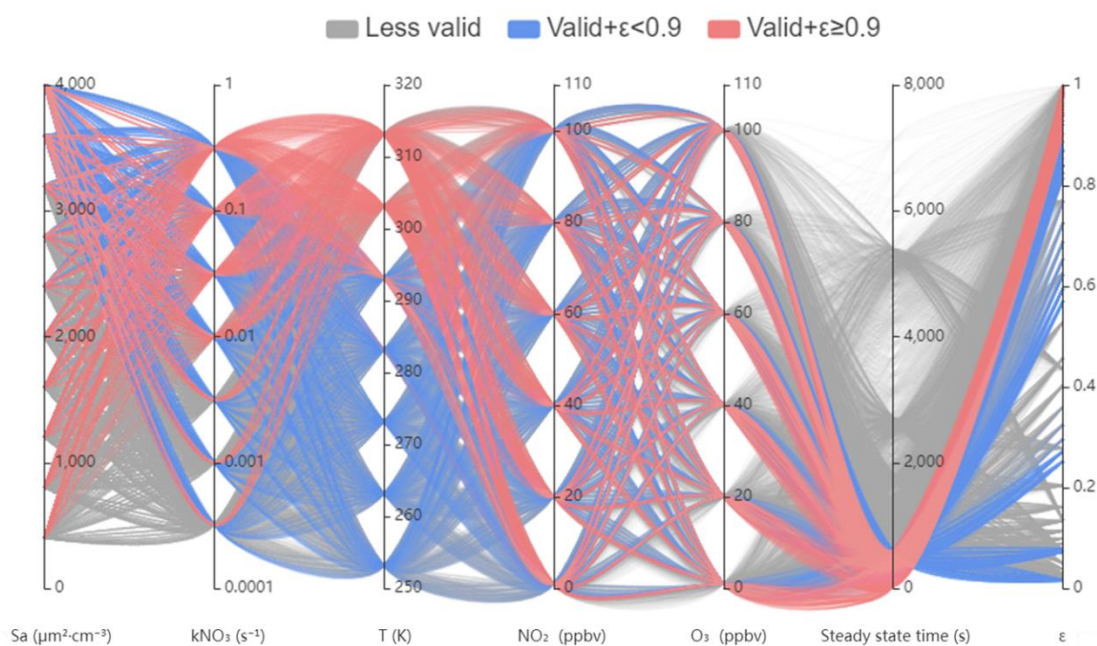
261 Besides the large variation of $k\text{NO}_3$ in short time period, the absolute level of $k\text{NO}_3$ and
262 $k\text{N}_2\text{O}_5$ could influence the possibilities of inaccurate $\gamma_{\text{ss}}(\text{N}_2\text{O}_5)$ from different aspects.
263 Although the enhancement of $k\text{NO}_3$ and $k\text{N}_2\text{O}_5$ boost the approach to steady state (Text. S5
264 and Figure S8), higher levels of $k\text{NO}_3$ amplify the bias of $\gamma_{\text{ss}}(\text{N}_2\text{O}_5)$, contrary to $k\text{N}_2\text{O}_5$, with
265 the same relative variation of $k\text{NO}_3$ (Text. S6 and Figure S10). It indicates that the region with
266 plural emissions (e.g. strong biogenic or vehicular emission) might not be suited for steady
267 state fit due to the high $k\text{NO}_3$. Therefore, a trade-off between the variation of $k\text{NO}_3$ and the
268 high level of $k\text{NO}_3$ (fast approach to steady state) should be made when derive $\gamma_{\text{ss}}(\text{N}_2\text{O}_5)$.

269 **3.3 Implication for accurate steady state analysis of $\text{NO}_3\text{-N}_2\text{O}_5$**

270 While a few studies have examined the validity of steady state under certain conditions via
271 numerical modeling when interpreted the ambient data (Brown et al., 2009; Brown et al., 2003),
272 a clear range well suited to steady state analysis of $\text{NO}_3\text{-N}_2\text{O}_5$, taking both K_{eq} and validity of
273 steady state into consideration, has not been determined to date.

274 Here almost 20000 simulations are displayed in the parallel plot of Figure 4, where each
275 line connects 5 constraint parameters to the calculated steady state time and ϵ (the correction
276 factor for K_{eq} parameterization to match the exact ratio of $[\text{N}_2\text{O}_5]/([\text{NO}_2] \times [\text{NO}_3])$, detailed in
277 Eq.6). The gray traces represent the simulations could not match steady state within 600 s and
278 were defined as less valid cases here. By this definition, we intend to indicate that it is also
279 viable to apply steady state approximation on air mass, which requires more than 600 s to
280 match steady state, whereas the uncertainty caused therefrom could increase to some extent.
281 The pink and blue traces together represent the simulations could match valid steady state
282 within 600 s without consideration of K_{eq} deviation (in other word the value of ϵ).
283 Furthermore, the criterion to apply steady state approximation appropriately we defined is that
284 approach to steady state within 600 s and the ϵ larger than 0.9, which are indicated as pink
285 traces. While the level of T , NO_2 and O_3 have minor effect on the approach to steady state,
286 simultaneous low $k\text{N}_2\text{O}_5$ (indicated as low Sa in the plot) and $k\text{NO}_3$ prevent the $\text{NO}_3\text{-N}_2\text{O}_5$
287 system from developing steady state. For example, when $k\text{NO}_3$ is lower than 0.01 s^{-1} , the air
288 mass will be valid only if Sa increases to at least $3000 \mu\text{m}^2 \text{ cm}^{-3}$ with $\gamma(\text{N}_2\text{O}_5)$ of 0.02. It implies
289 that clean air mass is not suited for steady state in any cases, whereas high aerosol condition
290 provides more possibilities to approach steady state even with low $k\text{NO}_3$. However, in order

291 to interpreting $\text{NO}_3\text{-N}_2\text{O}_5$ chemistry with accurate K_{eq} coefficient, the ϵ larger than 0.9 is
 292 additionally taken into consideration, which excludes 50% of valid steady state cases mainly
 293 with high aerosol and lower than 10°C . These cases could bias $[\text{N}_2\text{O}_5]/([\text{NO}_2]\times[\text{NO}_3])$ from
 294 original K_{eq} (also indicated in Figure 2), leading to inaccurate results of calculation based on
 295 K_{eq} .



296 **Figure 4.** Numerical simulations for determining conditions available for steady state approximation
 297 method in a parallel axis plot. Each line simply represents a simulation associated with different parameters
 298 in different vertical axes. The first five axes from the left represent initial variables used for constraining
 299 the simulations respectively. The last two axes represent the time required for achieving steady state and the
 300 ϵ value calculated from the simulated results. The gray lines show cases approaching steady state longer
 301 than 600 s (less valid). The blue lines show cases approaching steady state cases within 600 s while with ϵ
 302 less than 0.9, which is also inappropriate for steady state analysis. The pink lines show cases approaching
 303 steady state cases within 600 s with ϵ higher than 0.9, which is suited for steady state analysis.
 304

305 4 Conclusions

306 In this study, we found that the parameterized K_{eq} coefficient deviates much from the ratio of
 307 $[\text{N}_2\text{O}_5]/([\text{NO}_2]\times[\text{NO}_3])$ in some cases where steady state is valid. The indicator of the deviation,
 308 ϵ , is relatively sensitive to N_2O_5 reactivity and ambient temperature. It implies that conditions
 309 suited for steady state analysis should be determined according to not only the validity of
 310 steady state but also K_{eq} especially under high aerosol conditions, like some regions in India,
 311 China, Europe and the US (Baasandorj et al., 2017; Cesari et al., 2018; Huang et al.,
 312 2014; Mogno et al., 2021; Petit et al., 2017; Wang et al., 2017b). Considering that high level of

313 $k\text{NO}_3$ might amplify the bias of $\gamma_{\text{ss}}(\text{N}_2\text{O}_5)$ yield from steady state fit and appears to be
314 accompanied with fast variations, air mass of $k\text{NO}_3$ less than 0.01 s^{-1} with high aerosol and T
315 higher than 10°C is therefore the best suited for steady state analysis of $\text{NO}_3\text{-N}_2\text{O}_5$ chemistry,
316 which indicates that this method would be more applicable in polluted regions with high
317 aerosol loading during summertime. If the restriction of ε is relaxed to 30%, some of winter
318 conditions will also be applicable. Our results provide an insight to improve the accuracy of
319 steady state approximation method and find suited areas to interpret nighttime chemistry.
320 Further improvement of in-situ $\text{NO}_3\text{-N}_2\text{O}_5$ budgets quantification might relies on the direct
321 measurements via flow tube system or machine learning prediction based on ancillary
322 parameters.

323

324 **Supporting Information:** The Supporting Information is available on line.

325

326 **Code/Data availability.** The datasets used in this study are available from the corresponding
327 author upon request (wanghch27@mail.sysu.edu.cn; k.lu@pku.edu.cn).

328

329 **Author contributions.** K.D.L. and H.C.W. designed the study. X.R.C and H.C.W. analyzed
330 the data and wrote the paper with input from K.D.L.

331

332 **Competing interests.** The authors declare that they have no conflicts of interest.

333

334 **Acknowledgments.** This project is supported by the National Natural Science Foundation of
335 China (21976006, 42175111); the Beijing Municipal Natural Science Foundation for
336 Distinguished Young Scholars (JQ19031); National State Environmental Protection Key
337 Laboratory of Formation and Prevention of Urban Air Pollution Complex (CX2020080578);
338 the special fund of the State Key Joint Laboratory of Environment Simulation and Pollution
339 Control (21K02ESPCP); the National Research Program for Key Issue in Air Pollution
340 Control (DQGG0103-01, 2019YFC0214800). Thanks for the data contributed by field
341 campaign team.

342

343 **References**

344 Allan, B. J., Carslaw, N., Coe, H., Burgess, R. A., and Plane, J. M. C.: Observations of the nitrate radical in the
345 marine boundary layer, *Journal of Atmospheric Chemistry*, 33, 129-154, Doi 10.1023/A:1005917203307, 1999.
346 Allan, B. J., McFiggans, G., Plane, J. M. C., Coe, H., and McFadyen, G. G.: The nitrate radical in the remote

347 marine boundary layer, *J. Geophys. Res.: Atmos.*, 105, 24191-24204, 10.1029/2000JD900314, 2000.

348 Baasandorj, M., Hoch, S. W., Bares, R., Lin, J. C., Brown, S. S., Millet, D. B., Martin, R., Kelly, K., Zarzana, K.

349 J., Whiteman, C. D., Dube, W. P., Tonnesen, G., Jaramillo, I. C., and Sohl, J.: Coupling between Chemical and

350 Meteorological Processes under Persistent Cold-Air Pool Conditions: Evolution of Wintertime PM_{2.5} Pollution

351 Events and N₂O₅ Observations in Utah's Salt Lake Valley, *Environmental Science & Technology*, 51, 5941-5950,

352 10.1021/acs.est.6b06603, 2017.

353 Brown, S. S.: Applicability of the steady state approximation to the interpretation of atmospheric observations of

354 NO₃ and N₂O₅, *J. Geophys. Res.*, 108, 10.1029/2003jd003407, 2003.

355 Brown, S. S., Stark, H., and Ravishankara, A. R.: Applicability of the steady state approximation to the

356 interpretation of atmospheric observations of NO₃ and N₂O₅, *Journal of Geophysical Research-Atmospheres*,

357 108, Artn 4539

358 Doi 10.1029/2003jd003407, 2003.

359 Brown, S. S., Ryerson, T. B., Wollny, A. G., Brock, C. A., Peltier, R., Sullivan, A. P., Weber, R. J., Dube, W. P.,

360 Trainer, M., Meagher, J. F., Fehsenfeld, F. C., and Ravishankara, A. R.: Variability in nocturnal nitrogen oxide

361 processing and its role in regional air quality, *Science*, 311, 67-70, DOI 10.1126/science.1120120, 2006.

362 Brown, S. S., Dube, W. P., Fuchs, H., Ryerson, T. B., Wollny, A. G., Brock, C. A., Bahreini, R., Middlebrook, A.

363 M., Neuman, J. A., Atlas, E., Roberts, J. M., Osthoff, H. D., Trainer, M., Fehsenfeld, F. C., and Ravishankara, A.

364 R.: Reactive uptake coefficients for N₂O₅ determined from aircraft measurements during the Second Texas Air

365 Quality Study: Comparison to current model parameterizations, *J. Geophys. Res.- Atmos.*, 114, D00F10(01-16),

366 Artn D00f10

367 10.1029/2008jd011679, 2009.

368 Brown, S. S., Dubé, W. P., Peischl, J., Ryerson, T. B., Atlas, E., Warneke, C., de Gouw, J. A., te Lintel Hekkert,

369 S., Brock, C. A., Flocke, F., Trainer, M., Parrish, D. D., Fehsenfeld, F. C., and Ravishankara, A. R.: Budgets for

370 nocturnal VOC oxidation by nitrate radicals aloft during the 2006 Texas Air Quality Study, *J. Geophys. Res.:*

371 *Atmos.*, 116, 10.1029/2011jd016544, 2011.

372 Cantrell, C., Davidson, J., McDaniel, A., Shetter, R., and Calvert, J.: The equilibrium constant for N₂O₅ = NO₂

373 + NO₃ - Absolute determination by direct measurement from 243 to 397 K, *The Journal of Chemical Physics*,

374 88, 10.1063/1.454679, 1988.

375 Carslaw, N., Plane, J. M. C., Coe, H., and Cuevas, E.: Observations of the nitrate radical in the free troposphere

376 at Izana de Tenerife, *J. Geophys. Res.- Atmos.*, 102, 10613-10622, 10.1029/96jd03512, 1997.

377 Cesari, D., De Benedetto, G. E., Bonasoni, P., Busetto, M., Dinoi, A., Merico, E., Chirizzi, D., Cristofanelli, P.,

378 Donato, A., Grasso, F. M., Marinoni, A., Pennetta, A., and Contini, D.: Seasonal variability of PM_{2.5} and PM₁₀

379 composition and sources in an urban background site in Southern Italy, *Science of the Total Environment*, 612,

380 202-213, 10.1016/j.scitotenv.2017.08.230, 2018.

381 Chen, X., Wang, H., Lu, K., Li, C., Zhai, T., Tan, Z., Ma, X., Yang, X., Liu, Y., Chen, S., Dong, H., Li, X., Wu,

382 Z., Hu, M., Zeng, L., and Zhang, Y.: Field Determination of Nitrate Formation Pathway in Winter Beijing,

383 *Environmental Science & Technology*, 54, 9243-9253, 10.1021/acs.est.0c00972, 2020.

384 Huang, R.-J., Zhang, Y., Bozzetti, C., Ho, K.-F., Cao, J.-J., Han, Y., Daellenbach, K. R., Slowik, J. G., Platt, S.

385 M., Canonaco, F., Zotter, P., Wolf, R., Pieber, S. M., Brun, E. A., Crippa, M., Ciarelli, G., Piazzalunga, A.,

386 Schwikowski, M., Abbaszade, G., Schnelle-Kreis, J., Zimmermann, R., An, Z., Szidat, S., Baltensperger, U.,

387 Haddad, I. E., and Prévôt, A. S. H.: High secondary aerosol contribution to particulate pollution during haze

388 events in China, *Nature*, 514, 218-222, 10.1038/nature13774, 2014.

389 Li, Z. Y., Xie, P. H., Hu, R. Z., Wang, D., Jin, H. W., Chen, H., Lin, C., and Liu, W. Q.: Observations of N₂O₅
390 and NO₃ at a suburban environment in Yangtze river delta in China: Estimating heterogeneous N₂O₅ uptake
391 coefficients, *J. Environ. Sci.*, 95, 248-255, 10.1016/j.jes.2020.04.041, 2020.

392 McDuffie, E. E., Fibiger, D. L., Dubé, W. P., Lopez-Hilfiker, F., Lee, B. H., Thornton, J. A., Shah, V., Jaeglé, L.,
393 Guo, H., Weber, R. J., Michael Reeves, J., Weinheimer, A. J., Schroder, J. C., Campuzano-Jost, P., Jimenez, J. L.,
394 Dibb, J. E., Veres, P., Ebben, C., Sparks, T. L., Wooldridge, P. J., Cohen, R. C., Hornbrook, R. S., Apel, E. C.,
395 Campos, T., Hall, S. R., Ullmann, K., and Brown, S. S.: Heterogeneous N₂O₅ Uptake During Winter: Aircraft
396 Measurements During the 2015 WINTER Campaign and Critical Evaluation of Current Parameterizations, *J.*
397 *Geophys. Res.: Atmos.*, 123, 4345-4372, 10.1002/2018jd028336, 2018.

398 McDuffie, E. E., Womack, C. C., Fibiger, D. L., Dube, W. P., Franchin, A., Middlebrook, A. M., Goldberger, L.,
399 Lee, B. H., Thornton, J. A., Moravek, A., Murphy, J. G., Baasandorj, M., and Brown, S. S.: On the contribution
400 of nocturnal heterogeneous reactive nitrogen chemistry to particulate matter formation during wintertime
401 pollution events in Northern Utah, *Atmos. Chem. Phys.*, 19, 9287-9308, 10.5194/acp-19-9287-2019, 2019.

402 Mentel, T. F., Bleilebens, D., and Wahner, A.: A study of nighttime nitrogen oxide oxidation in a large reaction
403 chamber - The fate of NO₂, N₂O₅, HNO₃, and O₃ at different humidities, *Atmos. Environ.*, 30, 4007-4020,
404 10.1016/1352-2310(96)00117-3, 1996.

405 Mogno, C., Palmer, P. I., Knote, C., Yao, F., and Wallington, T. J.: Seasonal distribution and drivers of surface
406 fine particulate matter and organic aerosol over the Indo-Gangetic Plain, *Atmos. Chem. Phys.*, 21, 10881-10909,
407 10.5194/acp-21-10881-2021, 2021.

408 Morgan, W. T., Ouyang, B., Allan, J. D., Aruffo, E., Di Carlo, P., Kennedy, O. J., Lowe, D., Flynn, M. J.,
409 Rosenberg, P. D., Williams, P. I., Jones, R., McFiggans, G. B., and Coe, H.: Influence of aerosol chemical
410 composition on N₂O₅ uptake: airborne regional measurements in northwestern Europe, *Atmospheric Chemistry*
411 *and Physics*, 15, 973-990, DOI 10.5194/acp-15-973-2015, 2015.

412 Osthoff, H. D., Sommariva, R., Baynard, T., Pettersson, A., Williams, E. J., Lerner, B. M., Roberts, J. M., Stark,
413 H., Goldan, P. D., Kuster, W. C., Bates, T. S., Coffman, D., Ravishankara, A. R., and Brown, S. S.: Observation
414 of daytime N₂O₅ in the marine boundary layer during New England Air Quality Study - Intercontinental
415 Transport and Chemical Transformation 2004, *Journal of Geophysical Research-Atmospheres*, 111, Artn D23s14
416 10.1029/2006jd007593, 2006.

417 Petit, J. E., Amodeo, T., Meleux, F., Bessagnet, B., Menut, L., Grenier, D., Pellan, Y., Oekler, A., Rocq, B., Gros,
418 V., Sciare, J., and Favez, O.: Characterising an intense PM pollution episode in March 2015 in France from multi-
419 site approach and near real time data: Climatology, variabilities, geographical origins and model evaluation,
420 *Atmospheric Environment*, 155, 68-84, 10.1016/j.atmosenv.2017.02.012, 2017.

421 Phillips, G. J., Thieser, J., Tang, M., Sobanski, N., Schuster, G., Fachinger, J., Drewnick, F., Borrmann, S.,
422 Bingemer, H., Lelieveld, J., and Crowley, J. N.: Estimating N₂O₅ uptake coefficients using ambient measurements
423 of NO₃, N₂O₅, ClNO₂ and particle-phase nitrate, *Atmos. Chem. Phys.*, 16, 13231-13249, 10.5194/acp-16-13231-
424 2016, 2016.

425 Platt, U., Perner, D., Schroder, J., Kessler, C., and Toennissen, A.: The Diurnal-Variation of NO₃, *J Geophys Res-*
426 *Oceans*, 86, 1965-1970, DOI 10.1029/JC086iC12p11965, 1981.

427 Platt, U. F., Winer, A. M., Biermann, H. W., Atkinson, R., and Pitts, J. N.: Measurement of nitrate radical
428 concentrations in continental air, *Environmental Science & Technology*, 18, 365-369, 10.1021/es00123a015,
429 1984.

430 Pritchard, H.: The nitrogen pentoxide dissociation equilibrium, *Int. J. Chem. Kinet.*, 26, 61-71,

431 10.1002/kin.550260108, 1994.

432 Stutz, J., Alicke, B., Ackermann, R., Geyer, A., White, A., and Williams, E.: Vertical profiles of NO₃, N₂O₅, O-

433 3, and NO_x in the nocturnal boundary layer: 1. Observations during the Texas Air Quality Study 2000, *J. Geophys.*

434 *Res.- Atmos.*, 109, 10.1029/2003jd004209, 2004.

435 Vrekoussis, M., Mihalopoulos, N., Gerasopoulos, E., Kanakidou, M., Crutzen, P. J., and Lelieveld, J.: Two-years

436 of NO₃ radical observations in the boundary layer over the Eastern Mediterranean, *Atmospheric Chemistry and*

437 *Physics*, 7, 315-327, 2007.

438 Wagner, N. L., Riedel, T. P., Young, C. J., Bahreini, R., Brock, C. A., Dubé, W. P., Kim, S., Middlebrook, A. M.,

439 Öztürk, F., Roberts, J. M., Russo, R., Sive, B., Swarthout, R., Thornton, J. A., VandenBoer, T. C., Zhou, Y., and

440 Brown, S. S.: N₂O₅ uptake coefficients and nocturnal NO₂ removal rates determined from ambient wintertime

441 measurements, *J. Geophys. Res.: Atmos.*, 118, 9331-9350, 10.1002/jgrd.50653, 2013.

442 Wahner, A., Mentel, T. F., Sohn, M., and Stier, J.: Heterogeneous reaction of N₂O₅ on sodium nitrate aerosol, *J.*

443 *Geophys. Res.: Atmos.*, 103, 31103-31112, 10.1029/1998jd100022, 1998.

444 Wang, H., Lu, K., Chen, X., Zhu, Q., Chen, Q., Guo, S., Jiang, M., Li, X., Shang, D., Tan, Z., Wu, Y., Wu, Z.,

445 Zou, Q., Zheng, Y., Zeng, L., Zhu, T., Hu, M., and Zhang, Y.: High N₂O₅ Concentrations Observed in Urban

446 Beijing: Implications of a Large Nitrate Formation Pathway, *Environ Sci Tech Let*, 4, 416-420,

447 10.1021/acs.estlett.7b00341, 2017a.

448 Wang, H., Chen, X., Lu, K., Hu, R., Li, Z., Wang, H., Ma, X., Yang, X., Chen, S., Dong, H., Liu, Y., Fang, X.,

449 Zeng, L., Hu, M., and Zhang, Y.: NO₃ and N₂O₅ chemistry at a suburban site during the EXPLORE-YRD

450 campaign in 2018, *Atmospheric Environment*, 224, 10.1016/j.atmosenv.2019.117180, 2020a.

451 Wang, H., Chen, X., Lu, K., Tan, Z., Ma, X., Wu, Z., Li, X., Liu, Y., Shang, D., Wu, Y., Zeng, L., Hu, M., Schmitt,

452 S., Kiendler-Scharr, A., Wahner, A., and Zhang, Y.: Wintertime N₂O₅ uptake coefficients over the North China

453 Plain, *Science Bulletin*, 65, 765-774, 10.1016/j.scib.2020.02.006, 2020b.

454 Wang, H. C., Lu, K. D., Guo, S., Wu, Z. J., Shang, D. J., Tan, Z. F., Wang, Y. J., Le Breton, M., Lou, S. R., Tang,

455 M. J., Wu, Y. S., Zhu, W. F., Zheng, J., Zeng, L. M., Hallquist, M., Hu, M., and Zhang, Y. H.: Efficient N₂O₅

456 uptake and NO₃ oxidation in the outflow of urban Beijing, *Atmos. Chem. Phys.*, 18, 9705-9721, 10.5194/acp-

457 18-9705-2018, 2018.

458 Wang, J., Zhao, B., Wang, S., Yang, F., Xing, J., Morawska, L., Ding, A., Kulmala, M., Kerminen, V.-M.,

459 Kujansuu, J., Wang, Z., Ding, D., Zhang, X., Wang, H., Tian, M., Petäjä, T., Jiang, J., and Hao, J.: Particulate

460 matter pollution over China and the effects of control policies, *Sci. Total Environ.*, 584-585, 426-447,

461 <https://doi.org/10.1016/j.scitotenv.2017.01.027>, 2017b.

462 Wang, S., Shi, C., Zhou, B., Zhao, H., Wang, Z., Yang, S., and Chen, L.: Observation of NO₃ radicals over

463 Shanghai, China, *Atmos. Environ.*, 70, 401-409, 10.1016/j.atmosenv.2013.01.022, 2013.

464 Wang, X., Wang, H., Xue, L., Wang, T., Wang, L., Gu, R., Wang, W., Tham, Y. J., Wang, Z., Yang, L., Chen, J.,

465 and Wang, W.: Observations of N₂O₅ and ClNO₂ at a polluted urban surface site in North China: High N₂O₅

466 uptake coefficients and low ClNO₂ product yields, *Atmos. Environ.*, 156, 125-134,

467 10.1016/j.atmosenv.2017.02.035, 2017c.

468 Wang, Y., Yao, L., Wang, L., Liu, Z., Ji, D., Tang, G., Zhang, J., Sun, Y., Hu, B., and Xin, J.: Mechanism for the

469 formation of the January 2013 heavy haze pollution episode over central and eastern China, *Science China Earth*

470 *Sciences*, 57, 14-25, 10.1007/s11430-013-4773-4, 2014.

471 Wang, Z., Wang, W., Tham, Y. J., Li, Q., Wang, H., Wen, L., Wang, X., and Wang, T.: Fast heterogeneous N₂O₅

472 uptake and ClNO₂ production in power plant and industrial plumes observed in the nocturnal residual layer over

473 the North China Plain, *Atmos. Chem. Phys.*, 17, 12361-12378, 10.5194/acp-17-12361-2017, 2017d.
474 Yan, C., Tham, Y. J., Zha, Q. Z., Wang, X. F., Xue, L. K., Dai, J. N., Wang, Z., and Wang, T.: Fast heterogeneous
475 loss of N₂O₅ leads to significant nighttime NO_x removal and nitrate aerosol formation at a coastal background
476 environment of southern China, *Science of the Total Environment*, 677, 637-647,
477 10.1016/j.scitotenv.2019.04.389, 2019.
478 Yu, C., Wang, Z., Xia, M., Fu, X., Wang, W., Yee Jun, T., Chen, T., Zheng, P., Li, H., Shan, Y., Wang, X., Xue,
479 L., Zhou, Y., Yue, D., Ou, Y., Gao, J., Lu, K., Brown, S., Zhang, Y., and Tao, W.: Heterogeneous N₂O₅ reactions
480 on atmospheric aerosols at four Chinese sites: improving model representation of uptake parameters, *Atmos.*
481 *Chem. Phys.*, 20, 4367-4378, 10.5194/acp-20-4367-2020, 2020.
482